An analysis of the synchrotron radiation images of runaway electron beams in JET: island-like patterns and (partial) current collapse

C. Sommariva[1], A. Pau[1], S. Silburn[2], C. Reux[3], O. Ficker[4], M. Fontana[2], P. Carvalho[5], M. Hoppe[6], U. Sheikh[1], J. Decker[1], J.P. Graves[1], G. Pautasso[7], C.Paz-Soldan[8,9] and JET Contributors[2,*]

[1] *Ecole Polytechnique Fédérale de Lausanne (EPFL), Swiss Plasma Center (SPC), CH-1015, Lausanne, Switzerland*

[2] *EUROfusion Consortium, JET Culham Science Center, Abingdon, OX14 3DB, United Kingdom*

[3] *CEA, IRFM, F-12108, Saint-Paul-lez-Durance, France*

[4] *Institute of Plasma Physics of the CAS, CZ-18200, Praha 8, Czechia*

[5] *Instituto de Plasmas e Fusão Nuclear, Instituto Superior Técnico, Universidade Técnica de Lisboa, 1049-001 Lisboa, Portugal*

[6] *Department of Physics, Chalmers University of Technology, Göteborg, Sweden*

[7] *Max-Planck-Institute für Plasmaphysiks, D-85748, Garching, Germany*

[8] *General Atomics, PO Box 85608, San Diego, CA 92186-5608, USA*

[9] *Department of Applied Physics and Applied Mathematics, Columbia University, New York, NY 10024, USA*

[*] *See the author list of 'Overview of JET results for optimising ITER operation' by J. Mailloux et al. to be published in Nuclear Fusion Special Issue: Overview and Summary Papers from the 28th Fusion Energy Conference (Nice, France, 10-15 May 2021)*

Introduction

Runway electron (RE) beams are high-current highly relativistic electron beams which may be observed after a tokamak plasma disruption [1]. If generated, an uncontrolled RE beam strike may cause damage to the reactor first wall such as localised melting [1]. Therefore, the development of an effective RE mitigation scheme is of paramount importance for safe tokamak operations [2]. The RE mitigation method chosen for ITER is the Shattered Pellet Injection (SPI) [3] which consists of the injection of D_2 and heavy impurity mixtures via fragmented pellets [4]. Pellet fragmentation is obtained by introducing a bend in the injection barrel just before the nozzle [4]. The mitigation of RE beam via SPI has been tested in both the DIII-D and the JET tokamaks [5-6]. In this paper, the attention is focused on the RE mitigation experiments via SPI conducted in JET. More specifically, the paper discusses: 1) the dynamics of the total emission seen by the JET bolometers, IR and fast visible cameras, 2) the analysis of island-like patterns observed in the RE beam synchrotron emission and 3) the patterns visible during a RE beam (partial) current collapse. The pulses considered hereafter are: 95135, 95775, 95776 and 95137. In all four pulses, the RE beam was generated by triggering a disruption via Argon Massive Gas Injection (Ar-MGI) after 8s from the plasma breakdown. RE-beam mitigation via the SPI (barrel A-12.5mm) with pure D_2 and D_2-Neon (D_2-Ne) mixtures has been performed in pulses 95135, 95775 and 95776. Similarly, an attempt of mitigating a RE beam using the SPI (barrel C-4mm) with a pure D_2 pellet has been tried in pulse 95137 but failed. Therefore, pulse 95137 is used for comparing SPI mitigated and unmitigated RE beams. The pre-disruption plasma parameters are reported in tab. 1:

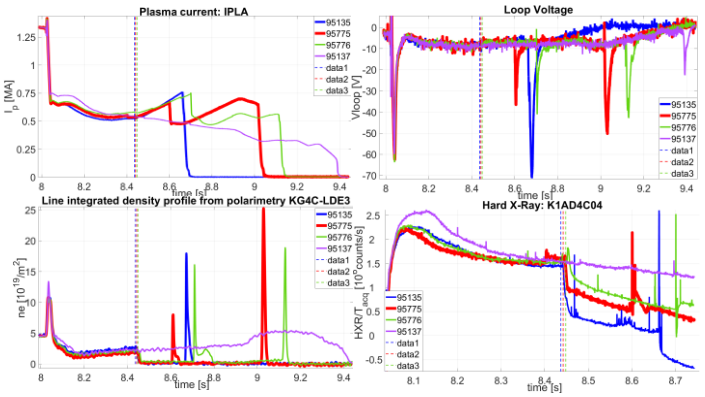

Figure 1 Profiles during the RE phase of pulses 95135 (in blue), 95775 (in red), 95776 (in green) and 95137 (in violet). From top left to bottom right: plasma current, loop voltage, integrated line density and HXR count rate. Dashed lines show the SPI arrival time for pulses 95135 (blue), 95775 (red) and 95776 (green).

Pulse	B_t [T]	I_p [MA]	n_e [m^{-2}]	T_e [keV]	MGI (Ar) [b]	SPI bar, pellet	SPI Ne [%]
95135	3	1.46	$4.2 \cdot 10^{19}$	2.5	0.12	A, broken pellet	0%
95775	3	1.46	$3.5 \cdot 10^{19}$	2.7	0.18	A, broken pellet	10%
95776	3	1.46	$4.1 \cdot 10^{19}$	2.6	0.18	A, good pellet	20%
95137	3	1.46	$4.1 \cdot 10^{19}$	2.6	0.12	C, no pellet	0%

Table 1 Main pulse parameters. The pre-disruption plasma parameters are taken at 6.5s after breakdown. The core line-integrated density (n_e) and the electron temperature (T_e) are obtained via polarimetry and ECE diagnostics.

The plasma current (top-left), loop voltage (top-right), line-integrated density (LID, bottom left) and hard X-Ray count rate (HXR, bottom-right) profiles recorded during the RE phase of pulses 95135 (in blue), 95775 (in red), 95776 (in green) and 95137 (in violet) are reported in fig.1. While profiles of the 4 pulses behave similarly before the SPI (~8.4s) striking differences appear afterwards. A drop in the LID and HXR count rate is observed after the SPI arrival (~8.45s). A reduction of the loop voltage w.r.t. the non-mitigated case is observed as well. The reduction of LID, HXR and loop voltage signals indicates that the Ar impurities, introduced via MGI, have been flushed out by the injection of large D_2 quantities. Conversely, the beam current increases almost linearly in time after the SPI and after the partial current collapse probably due to the restoring action of the control system. Indeed, the reference plasma current for the pulses considered here is of 1.5MA. The increase of beam current is interrupted by a sudden drop in the current itself probably due to MHD instabilities. It is worth noting that spikes in the LID, HXR and loop voltage signals are observed during a RE current collapse which indicate that: 1) a background plasma is ionized and 2) RE are deconfined. Different amounts of Ne lead to different post-collapse behaviour of the RE beam. Full RE dissipation is obtained for pure D_2-SPI (95135) [7], a second current increase collapse cycle is observed for a 10%Ne pellets (95775) while RE dissipation is not achieved for D_2-20%Ne pellet, (95776).

Overview JET RE beam synchrotron radiation

RE beam synchrotron radiation can be observed by the JET fast visible (λ~400-700nm) and IR (λ~3-3.5μm) cameras [8]. Examples of IR and fast visible images of the pulse 95135 RE beam are given in fig. 2 (top). The total number of counts per frame for the IR and the fast visible cameras are reported respectively at the bottom-left and bottom-right of fig. 2. As observed in fig. 1, the emission profiles of RE beams mitigated with D_2-rich SPI (95135 in blue, 95775 in red and 95776 in green) differ significantly from the non-mitigated ones (95137 in violet). After a first initial phase common to all pulses, the emission received by the cameras from the non-mitigated RE beam decreases almost linearly in time. Conversely, a fast drop in the received emission is observed for mitigated RE beams. It is worth noting that the integrated emission from the visible system promptly increases during the current collapses and the SPI arrival. This is a sign of possible light pollution from D and Ne radiation. The IR camera seems to be unaffected by D/Ne emissions (no increase during the shard injection and intensity drop during collapse). Changes in radiation patterns can also be identified by

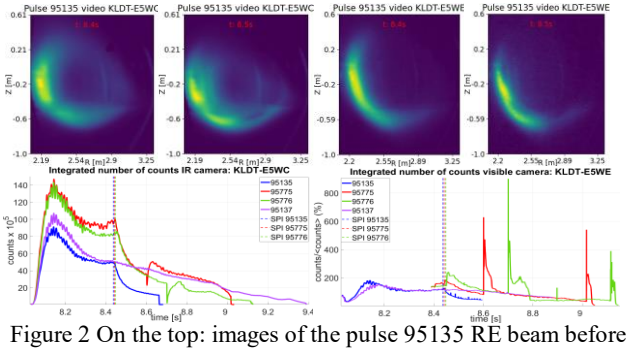

Figure 2 On the top: images of the pulse 95135 RE beam before (8.4s) and after (8.5s) the SPI: IR and fast visible images are denoted respectively with: KLDT-E5WC and KLDT-E5WE. At the bottom: integrated number of counts for the IR (left plot) and fast visible (right plot) cameras. Blue, red, green and violet lines are associated with the pulses 95135, 95775, 95776 and 95137. Dashed lines indicate the shard arrival time.

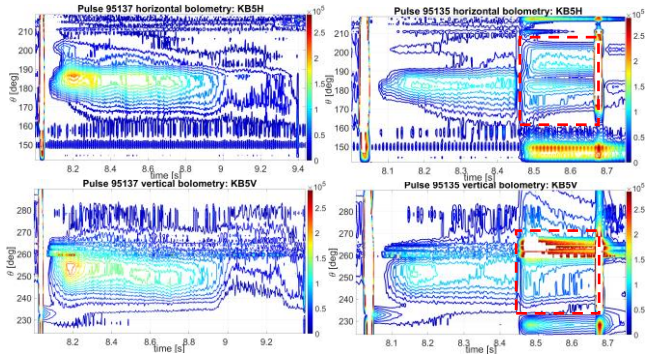

Figure 3 Line integrated radiation power density as received by the horizontal (top) and vertical (bottom) bolometers for non-mitigated (left) and D2 SPI mitigated (right) RE beams. Post-SPI RE beams are indicated with red squares (dashed lines). The line integrated radiation power density is reported in W/m^2.

the horizontal (fig. 3 top row) and vertical (fig. 3, bottom row) bolometers. Fig. 3 compares the line integrated radiation power density for the unmitigated (left column-95137) and the D2-mitigated (right column-95135) RE beams. As for the camera system, differences between pulse 95137 and 95135 radiation patterns are mainly found after the D_2-SPI. Indeed, a direct comparison between non-mitigated and D_2-mitigate RE pulses shows lower emission levels after the SPI which continuously decrease until beam collapse (contraction of the emission patters). Trends in the bolometer measurements are with the IR and fast visible camera. Considering the beam synchrotron radiation as the dominant light source during the RE phase of the discharge, the reduction of received radiation indicates a possible decrease of the RE energy and variations in the RE pitch angle [9]. Indeed, SOFT simulations suggest that the drop in the synchrotron radiation intensity is not reduced by the beam downward VDE [10,11]. Effects due to changes in the magnetic field may also be excluded because inconsistent with the increase of the plasma current (magnetic field) and the common trends seen by diagnostics (camera and bolometers) looking at the beam from different directions.

Island-like patterns

During the 2018-2020 JET RE experiments, island-like patterns having identifiable poloidal mode number (m) have been observed in both IR and visible synchrotron radiation images for approximately 61% of the RE beams and for multiple times for each beam. Multiple chains of island patterns have been observed to co-exist as well. The pattern dynamics can be analysed using computer vision codes such as the JET Particle Video Tracker (JPVT) originally developed for tracking SPI shards [12]. Fig. 4 reports the analysis of the m=5 patterns observed in pulse 95775 between 8.4015s and 8.45s using JPVT. Images capturing different phases of the pattern evolution are reported in the top and center-left plots while their estimated radial position, rotation frequency and island width are respectively reported in the center-right, bottom-left and bottom-right plots. As visible in fig. 4, the m=5 pattern chain initially appears at the RE beam core for promptly moving at approximately 75% of the beam minor radius. Successively, the pattern chain radial position shrinks in time until disappearing at approximately 35% of the beam minor radius. The rotation frequency of the m=5 patterns is found not to be constant in time. Indeed, cycles of angular acceleration (up to ~1.1kHz) followed by prompt locking are observed. The pattern width is estimated to be within 10% and 25% of the beam minor radius.

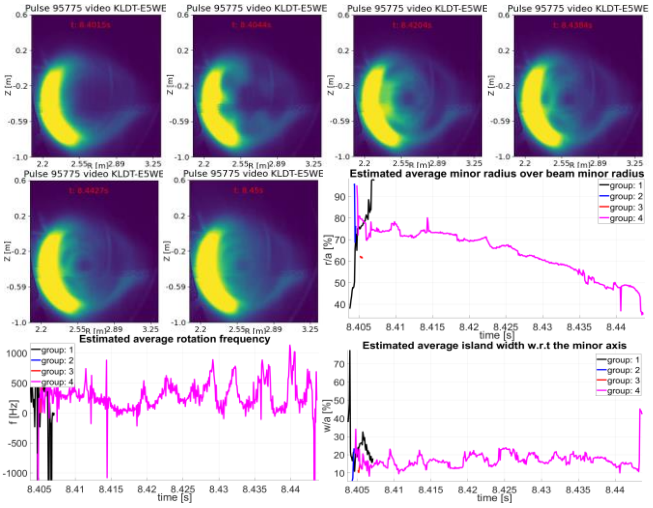

Figure 4 Island-like patterns visible in pulse 95775 between 8.4015s and 8.45s. From top to center left: pattern images as seen by the JET fast visible camera. From center to bottom right: estimated pattern radial position, rotation frequency and width.

Runaway Electron current collapse

Pattens in the visible RE beam radiation have been observed during the RE partial collapse of the pulse 95775. A first example is the presence of island-like patterns having poloidal mode number m=5 (outer chain) and m=4 (inner chain) anticipating the beam collapse. The m=5 and m=4 patterns are highlighted respectively by dashed magenta and dashed red ellipses in the top left images of fig. 5. The estimated radial position, rotation frequency and width of the

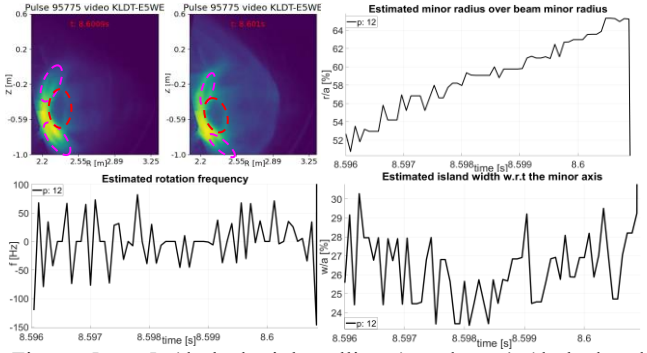

Figure 5 m=5 (dashed violet ellipses) and m=4 (dashed red ellipses) island-like patterns preceding the pulse 95775 partial collapse. Images of the precursors (fast visible camera) are reported in the top left plots. Top right, bottom left and bottom right plots report respectively the estimated m=4 radial position, rotation frequency and width.

m=4 chain are reported respectively in the top-right, bottom-left and bottom-right plots of fig. 5. The estimated radial position shows that the m=4 patterns are radially unstable and they move towards the beam edge. Beam collapse is triggered when the m=4 pattern reaches ~65% of the beam minor radius. Considering the bottom-left plot of fig. 5, no evident rotation frequency is observed (lock patterns). The m=4 pattern width is approximately 30% of the beam minor radius at collapse (fig. 5 bottom-right plot). Multiple features can be recognised in the visible images during the RE beam collapse (fig. 6). Correlations between visible features with spikes in the HXR count rate (fig. 6 top plot) are highlighted with bounding boxes of different colours. It worth noting that spikes in the HXR signals may be due to collisions between REs and the background plasma or direct RE losses. At first, we observe that the destabilization of the m=5 and m=4 pattern chains, leading to the beam collapse, correlates with a first spike in the HXR count rate (blue box). The flash observed at collapse is probably related to the reionisation of the background plasma. A second set of spikes in the HXR count rate profile correlates with the generation of a secondary radially unstable m=4 pattern chain (yellow boxes). The visible dynamics is 1) deformation of the beam core light patterns from a circular to a 'cross' structure, 2) separation of the 'cross' tips forming m=4 pattern chain, 3) radial motion of the m=4 pattern chain towards the beam edge until disappearance. A third set of spikes in the HXR signal is correlated with the collapse of a radiation belt seen approximately at the beam core (green boxes).

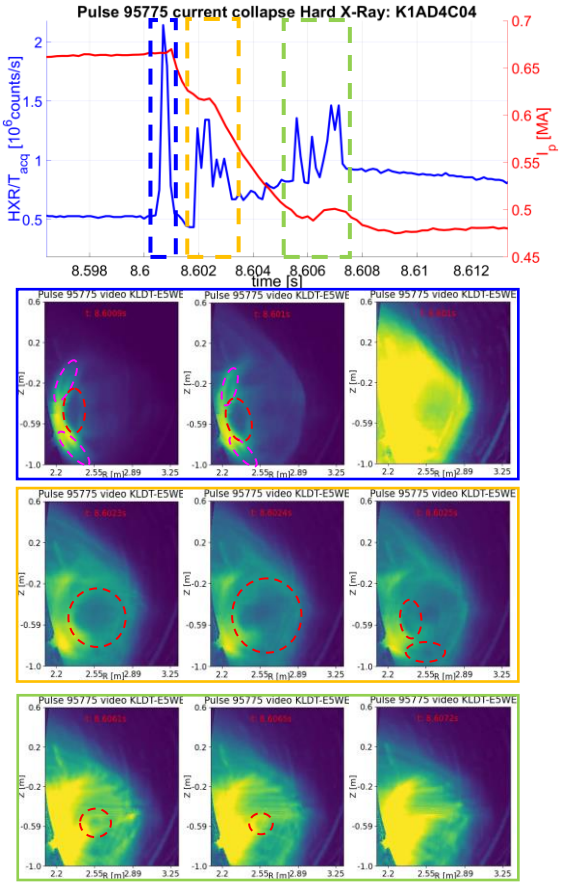

Figure 6 Features observed in images of the pulse 95775 partial RE beam collapse (visible camera). Top plot: HXR count rate (blue solid line) and plasma current (red solid line) profiles. Blue, red and green bounding boxes (dashed lines) relates the HXR spikes to the visible images. Red and magenta ellipses (dashed lines) identify features visible in images.

Conclusions

In this work, a first analysis of the radiation seen by the bolometers, IR and fast visible cameras of D_2-rich SPI mitigated RE beams is presented. All diagnostics found a decrease in the radiation signal after the SPI w.r.t non mitigated RE beams which is probably a sign of a drop in the RE energy. Island-like patterns have been observed in the synchrotron radiation of JET RE beams. Analysis of the m=5 pattern visible in pulse 95775 shows that fast changes in the patterns radial position and rotation frequency are possible. m=5 and m=4 island chains are seen as precursors of the pulse 95775 partial beam collapse. Spikes in the HXR count rate during the pulse 95775 partial collapse correlate with the dynamics of unstable m=4 patterns visible in the camera, and possible collapse of radiation belts.

Acknowledgments

This work has been carried out within the framework of the EUROfusion Consortium and has received funding from the Euratom research and training programme 2014-2018 and 2019-2020 under grant agreement No. 633053. The views and opinions expressed herein do not necessarily reflect those of the European Commission. This work was supported in part by the Swiss National Science Foundation.

Reference

[1] C. Reux et al., Nucl. Fusion, vol. 55, p. 093013, 2015
[2] E. M. Hollmann et al., Phys. of. Plasmas, vol. 22, p. 021802, 2015
[3] L. R. Baylor et al., Theory Sim. Disr. Workshop, Princeton, USA, 2018
[4] L. R. Baylor et al., Theory Sim. Disr. Workshop, Princeton, USA, 2017
[5] D. Shiraki et al., Nucl. Fusion, vol. 58, p. 056006, 2018
[6] C. Reux et al., oral contrib. to this conference, 2021
[7] C. Reux et al., Phys. Rev. Lett., vol. 126, p. 175001, 2021
[8] https://users.euro-fusion.org/openwiki/index.php/KL8
[9] J. Schwinger, Phys. Rev. vol. 75, p. 1912, 1949
[10] M. Hoppe et al., Nucl. Fusion, vol. 58, p. 026032, 2018
[11] O. Ficker et al, presentation at the JET M18-36 meeting, June 2021
[12] C. Sommariva et al., 61st APS DPP Meeting, 21-25 October 2019, Ft. Lauderdale, Florida USA